NASA/TM-20230009565

# Exploring the Langtry-Menter Transition Model for High Speed Applications Using FUN3D

*David J. Friedlander and Nicholas J. Georgiadis*
*Glenn Research Center, Cleveland, Ohio*

July 2023

# NASA STI Program . . . in Profile

Since its founding, NASA has been dedicated to the advancement of aeronautics and space science. The NASA Scientific and Technical Information (STI) Program plays a key part in helping NASA maintain this important role.

The NASA STI Program operates under the auspices of the Agency Chief Information Officer. It collects, organizes, provides for archiving, and disseminates NASA's STI. The NASA STI Program provides access to the NASA Technical Report Server—Registered (NTRS Reg) and NASA Technical Report Server—Public (NTRS) thus providing one of the largest collections of aeronautical and space science STI in the world. Results are published in both non-NASA channels and by NASA in the NASA STI Report Series, which includes the following report types:

- TECHNICAL PUBLICATION. Reports of completed research or a major significant phase of research that present the results of NASA programs and include extensive data or theoretical analysis. Includes compilations of significant scientific and technical data and information deemed to be of continuing reference value. NASA counter-part of peer-reviewed formal professional papers, but has less stringent limitations on manuscript length and extent of graphic presentations.

- TECHNICAL MEMORANDUM. Scientific and technical findings that are preliminary or of specialized interest, e.g., "quick-release" reports, working papers, and bibliographies that contain minimal annotation. Does not contain extensive analysis.

- CONTRACTOR REPORT. Scientific and technical findings by NASA-sponsored contractors and grantees.

- CONFERENCE PUBLICATION. Collected papers from scientific and technical conferences, symposia, seminars, or other meetings sponsored or co-sponsored by NASA.

- SPECIAL PUBLICATION. Scientific, technical, or historical information from NASA programs, projects, and missions, often concerned with subjects having substantial public interest.

- TECHNICAL TRANSLATION. English-language translations of foreign scientific and technical material pertinent to NASA's mission.

For more information about the NASA STI program, see the following:

- Access the NASA STI program home page at http://www.sti.nasa.gov

- E-mail your question to help@sti.nasa.gov

- Fax your question to the NASA STI Information Desk at 757-864-6500

- Telephone the NASA STI Information Desk at 757-864-9658

- Write to:
  NASA STI Program
  Mail Stop 148
  NASA Langley Research Center
  Hampton, VA 23681-2199

NASA/TM-20230009565

# Exploring the Langtry-Menter Transition Model for High Speed Applications Using FUN3D

*David J. Friedlander and Nicholas J. Georgiadis*
*Glenn Research Center, Cleveland, Ohio*

National Aeronautics and
Space Administration

Glenn Research Center
Cleveland, Ohio 44135

July 2023

## Acknowledgments

The authors would like to thank the NASA Transformational Tools and Technologies (TTT) Project for supporting this work and the NASA's High-End Computing Program for providing supercomputing resources.

This work was sponsored by the
Transformative Aeronautics Concepts Program.

*Level of Review*: This material has been technically reviewed by technical management.

This report is available in electronic form at https://www.sti.nasa.gov/ and https://ntrs.nasa.gov/

# Exploring the Langtry-Menter Transition Model for High Speed Applications Using FUN3D

David J. Friedlander and Nicholas J. Georgiadis
National Aeronautics and Space Administration
Glenn Research Center
Cleveland, Ohio 44135

## Abstract

A series of Reynolds-averaged Navier-Stokes (RANS) simulations were performed using the FUN3D flow solver to explore the capabilities of the Langtry-Menter Shear-Stress Transport (LM-SST) transition model for predicting transition for aircraft inlet applications. Two geometries were simulated: a zero-pressure-gradient flat plate and an axisymmetric cone exposed to hypersonic flow. In addition to the transition-sensitized LM-SST model investigations, simulations were run with the one-equation Spalart-Allmaras (SA) and the two-equation Menter Shear-Stress Transport (SST-V) RANS models in fully turbulent mode to identify the natural RANS model transition behavior as a function of Mach number when executed in fully turbulent mode. The flat plate simulations showed that (1) the transition model was able to predict rapid transition at a freestream Mach number of 0.2, which is expected but (2) the predicted transition location moved downstream as the freestream Mach number was increased for the simulations that used the SST-V turbulence model. The latter is significant as it is usually assumed that one- and two-equation turbulence models will produce fully turbulent flow very near the boundary layer origin. The flat plate simulation freestream Mach number trend was confirmed with simulations using the Wind-US code, which also saw a similar trend when employing the SA turbulence model. For the axisymmetric cone simulations, the transition location was highly sensitive to the inflow turbulence levels. This is significant as the prediction of the transition location is crucial when trying to predict inlet performance, especially for hypersonic vehicle applications. It was also noted that the predicted transition location for the cone when using the SST-V turbulence model agreed well with the predicted transition location from the equivalent zero-pressure-gradient cold wall flat plate case.

## 1.0 Nomenclature

| | |
|---|---|
| $c_f$ | skin friction coefficient |
| $c_p$ | specific heat at constant pressure |
| $h$ | enthalpy |
| $I$ | turbulence intensity |
| $k$ | turbulent kinetic energy |
| $L$ | axial length |
| $M$ | Mach number |
| $\dot{q}_w$ | wall heat flux |
| $\mathrm{Re}_x$ | Reynolds number |
| St | Stanton number |
| $s$ | distance from inflow plane to cone leading edge |
| $T_0$ | total temperature |
| $u$ | streamwise velocity |
| $x, y, z$ | Cartesian coordinates |

$y^+$ nondimensional wall distance
$\gamma$ turbulence intermittency
$\mu$ dynamic viscosity
$\rho$ density
$\omega$ specific turbulent dissipation rate

**Subscripts**
edge boundary layer edge
*in* inflow
tip cone tip
*t* turbulent
*w* wall
$\infty$ freestream

## 2.0 Introduction

There is an interest within the aviation community to incorporate more certification by analysis (Refs. 1 and 2), with a motivation to reduce flight and wind tunnel testing requirements, which are very costly for a new aircraft development program. More accurate simulation of the propulsion system was emphasized within the CFD 2030 Vision Study report as one of the proposed grand challenges (Ref. 3) in the field of computational aerodynamics. A major shortfall in the accuracy of all aerodynamic prediction techniques remains the prediction of turbulent flows. This also includes flows having boundary layers that transition from laminar to turbulent flow. In response to the report, the Transformational Tools and Technologies (TTT) project of the NASA Aeronautics Research Mission Directorate has focused on the development and validation of more accurate computational tools for simulating aerospace vehicles/components and predicting their performance (Ref. 4). While Reynolds-averaged Navier-Stokes (RANS) methods are still the practical state-of-the-art for most engineering-focused aerodynamic calculations, the TTT project has focused on scale resolving techniques, employing some form of large eddy simulation (LES) for turbulent flow predictions. For transitional flows, however, LES is not globally applicable, because the transition process is frequently dominated by amplification of very small disturbances which transition a laminar boundary layer to a turbulent state. A summary of transition mechanisms at high speeds is provided in Reference 5. On one end of the spectrum in transition mechanisms is modal growth (frequently referred to as “Tollmien-Schlichting mode growth”) which occurs in small-disturbance environments. On the other end, in high freestream disturbance environments, the pathway known as bypass transition usually occurs. By its very nature, LES does not typically capture the small scales which are responsible for low disturbance transition processes.

Therefore, within the class of boundary layer transition prediction for aerodynamic applications, RANS-based methods are still being investigated. For subsonic transport aircraft applications, transition prediction is of particular interest on the wings. The propulsion system also experiences transition in the inlet and frequently in the turbine stage within an engine core, although the modes of transition are different. For supersonic and hypersonic vehicles, transition in the inlet is of particular importance. Hypersonic vehicles typically have a forebody of the vehicle which serves as the initial part of the inlet compression system, and knowledge of the boundary layer transition is of paramount importance in predicting overall vehicle drag and inlet performance. To that goal, this paper investigates the ability of a popular RANS-based transition-sensitized model, the Langtry-Menter Shear-Stress Transport (LM-SST) formulation (Ref. 6) to determine its capability to predict transition for hypersonic aircraft inlet

applications. The geometries explored in this paper begin with a zero-pressure-gradient flat plate to benchmark the model. Next, an axisymmetric cone, representing the forebody of a hypersonic vehicle, is considered. Results using the transition model are compared with computations made using the one-equation Spalart-Allmaras (SA) (Ref. 7) and two-equation Menter Shear-Stress Transport (SST) (Ref. 8) turbulence models. The particular form of the SST model used in fully turbulent mode in this paper is that using the vorticity based turbulent production term, or SST-V. It is noted that traditional RANS models operated in "fully turbulent" mode still experience a transition of sorts. Typically, the boundary layer has a very short laminar region, and then turbulent production within the RANS models rapidly transitions the flow to fully turbulent mode. Part of this study explores the performance of these RANS models in fully turbulent mode to determine the "natural" transition behavior of these models as the freestream Mach number is increased.

## 3.0 Flow Solver and Transition Model

Most simulations were performed with the NASA's Fully Unstructured Navier-Stokes (FUN3D) code (Ref. 9), with a subset of "fully turbulent" turbulence model simulations performed with the NASA's Wind-US code (Ref. 10). The motivation for doing so was to verify the FUN3D results. Wind-US is a node-based, productional level code developed and maintained at the NASA Glenn Research Center. It can solve the 2D/3D Euler and RANS equations for incompressible and compressible flows on structured and unstructured grids. All Wind-US simulation results presented in this paper utilized the structured solver within Wind-US.

Like Wind-US, FUN3D is a node-based production level code that can solve the 2D/3D Euler and RANS equations for incompressible and compressible flows, however, it does so only on unstructured grids. The FUN3D flow solver is developed and maintained at the NASA Langley Research Center and was chosen for two primary reasons: (1) it can handle unstructured grids and (2) because it contains advanced turbulence models, and more recently transition models (Ref. 11). The transition model in FUN3D (Ref. 12) employs the SST k-ω formulation of Langtry and Menter (Ref. 6). In addition to solving the traditional RANS equations for the turbulent kinetic energy and specific turbulent dissipation rate, two additional transport equations are modelled to enable the simulation of transition. The two additional quantities that are solved are the turbulence intermittency, denoted by $\gamma$, and the transition Reynolds number based on momentum thickness denoted by $Re_{\theta t}$. The model was originally developed for problems characterized by bypass transition, i.e., when transition occurs where high freestream turbulence levels are experienced. For free flight conditions, where freestream turbulence is typically low, and where the transition process is typically due to the growth of Tollmien-Schlichting waves, it has been noted that RANS-sensitized models are being applied outside their original intended purpose. However, these models still have demonstrated some success, and in the absence of more generally applicable physics-based techniques, have shown to provide value in terms of preliminary engineering prediction tool capability.

For the specific class of hypersonic boundary layer prediction capability using RANS-sensitized models, there have been other studies in recent years. In Papp and Dash (Ref. 13), a k-ε based transition model, having an extra transport equation for intermittency, was solved in addition to the two traditional turbulent transport variable equations. The model was applied with success to several high Mach number cone problems. This model was extended to be more applicable to general three-dimensional problems in Papp and Dash (Ref. 14). Aliaga, et al. (Ref. 15) investigated the Langtry-Menter SST-based transition model in Ansys Fluent for flows around cones at approximately Mach 7 and flat plate boundary layers up

to Mach 11. References 16 to 19 also applied the Langtry-Menter SST-based transition model to hypersonic forebody flows.

# 4.0 Geometry and Numerical Modeling

## 4.1 2D Flat Plate

The 2D zero-pressure-gradient flat plate from the 1st AIAA Transition Modeling and Prediction Workshop (Ref. 20) was chosen for its simplicity as the starting point for testing the LM-SST transition model. The flat plate was run at the freestream condition outlined in Table I. As it will be discussed further in the Section 5.0, two sets of freestream turbulence levels were specified corresponding to a reference set of experimental data used extensively for transition model investigations. A family of 2D unstructured grids that were provided by the workshop were used to model the flat plate, with grid dimensions noted in Table II. The viscous spacing was such that the nominal $y^+$ was 1.872 for the first point off the wall on the workshop-denoted "tiny" grid level and 0.0486 on the extra extra fine grid level. The nominal $y^+$ values were based on the run condition outlined in Table I. A sample grid is shown in Figure 1. Boundary conditions included subsonic inflow (which specified total pressure and total temperature), farfield (which utilized Riemann invariants) on the upper boundary, and back pressure at the outflow. The lower boundary was divided into two parts: the flat plate which used an adiabatic viscous wall boundary condition and the portion upstream of the flat plate which used a z-plane symmetry boundary condition.

TABLE I.—2D FLAT PLATE MEAN FLOW RUN CONDITION

| | |
|---|---|
| Freestream Mach number | 0.2 |
| Reynolds number | $6.56\times10^5$ m$^{-1}$ |
| Total temperature | 302.4 K |

TABLE II.—NODE COUNTS FOR THE FLAT PLATE GRIDS

| | Nodes | | | |
|---|---|---|---|---|
| | j-Dim | | | |
| Grid level | Upstream[a] | Total | k-Dim | Total ($\times10^3$) |
| Tiny | 13 | 45 | 25 | 1.13 |
| Coarse | 25 | 89 | 49 | 4.36 |
| Medium | 49 | 177 | 97 | 17.17 |
| Fine | 97 | 353 | 193 | 68.13 |
| Extra fine | 193 | 705 | 385 | 271.43 |
| Extra extra fine | 385 | 1,409 | 769 | 1,083.52 |

[a]Includes the flat plate leading edge

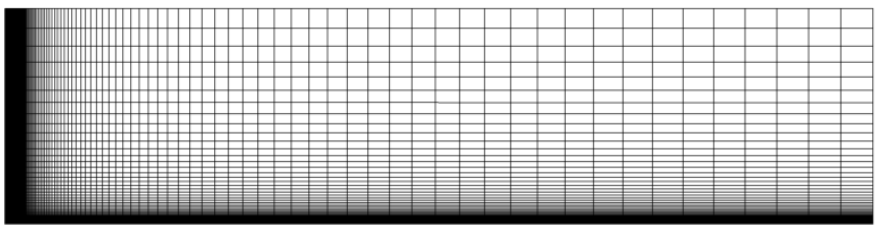

Figure 1.—Sample 2D flat plate grid (medium grid level).

## 4.2 Axisymmetric Cone

The higher speed geometry of interest for investigating the LM-SST model was an axisymmetric cone tested in the U.S. Air Force Arnold Engineering Development Center (AEDC) tunnel B by R. Kimmel (Ref. 21). The cone is 1016 mm in length with a half angle of 7°. The tip of the cone was rounded with a radius of 0.0381 mm. As reported in Reference 21, several versions of the cone were tested to vary the pressure gradient. The zero-pressure gradient version was chosen for simulation in this work to best compare against the zero-pressure gradient flat plate case.

A family of quarter-symmetry grids were generated using the Pointwise software (Ref. 22) to model the axisymmetric cone. The grid geometry consisted of the cone with a cylindrical downstream extension to turn the flow back to axial. To improve grid quality, the cone tip radius was increased to 2 mm. Viscous spacing was such that the nominal $y^+$ was 0.194 at the run condition outlined in Table III on the coarsest grid. The intent was to generate the grids using structured blocks, however the grid quality around the rounded cone tip became problematic. To solve that issue, a hybrid approach was taken in that region. This entailed creating structured blocks, with hexahedral shaped cells directly around the cone tip for capturing the boundary layer. Those blocks were then surrounded by an unstructured block with tetrahedral cells, which in turn was surrounded by structured-like blocks. A sample grid is shown in Figure 2 and the node counts for the generated grids are listed in Table IV. Boundary conditions included freestream at the inflow (which was specified via fluxes), farfield for the upper boundary, extrapolation at the outflow, and y- and z-symmetry planes. The cone was modeled as a nonadiabatic viscous wall with a wall temperature of 303.24 K. The wall temperature was set per the recommendation of Reference 21.

TABLE III.—AXISYMMETRIC CONE RUN CONDITION

| | |
|---|---|
| Freestream Mach number | 7.93 |
| Reynolds number | $6.60\times10^6$ m$^{-1}$ |
| Total temperature | 722.00 K |
| Wall temperature | 303.24 K |

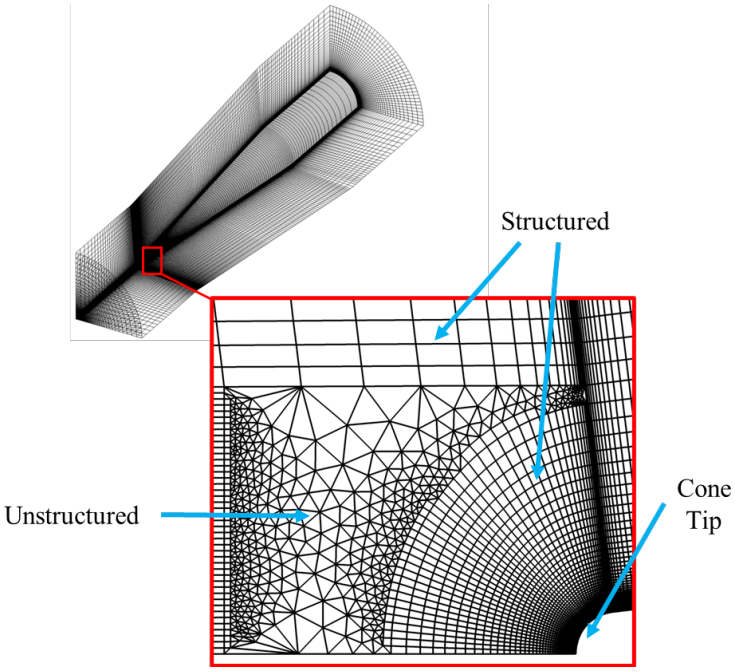


Figure 2.—Sample axisymmetric cone grid (coarse grid level).

# 5.0 Results

## 5.1 2D Flat Plate

A grid convergence study was performed that focused on the simulations that utilized the LM-SST transition model. Those simulations used the Roe flux construction scheme (Ref. 23) in conjunction with the Venkatakrishnan flux limiter (Ref. 24). The smooth limiter coefficient was set to one for the flux limiter. The grid convergence study was performed at two different turbulent inflow conditions, T3A and T3B (Ref. 25), which are outlined in Table V. From Figure 3 it can be seen that the skin friction coefficient profiles achieve grid independence at the extra fine grid level. This is true for both the T3A and T3B cases. It is also noted that the predicted transition location is in acceptable agreement with the experimental data. Although results of the workshop findings were not yet published at the time of this report, results obtained here for the LM-SST model were consistent with those submitted by workshop participants. These findings provided confidence to examine the transition model for a more complicated flow problem, the axisymmetric cone at nearly Mach 8 flow conditions.

TABLE IV.—NODE COUNTS FOR THE AXISYMMETRIC CONE GRIDS

| Grid level | Nodes ($\times 10^6$) |
|---|---|
| Coarse | 1.13 |
| Medium | 9.30 |
| Fine | 75.37 |

TABLE V.—2D FLAT PLATE TURBULENCE INFLOW CONDITIONS

| | $\mu_t/\mu$ | $I$, % |
|---|---|---|
| T3A | 11.9 | 5.855 |
| T3B | 99.0 | 7.216 |

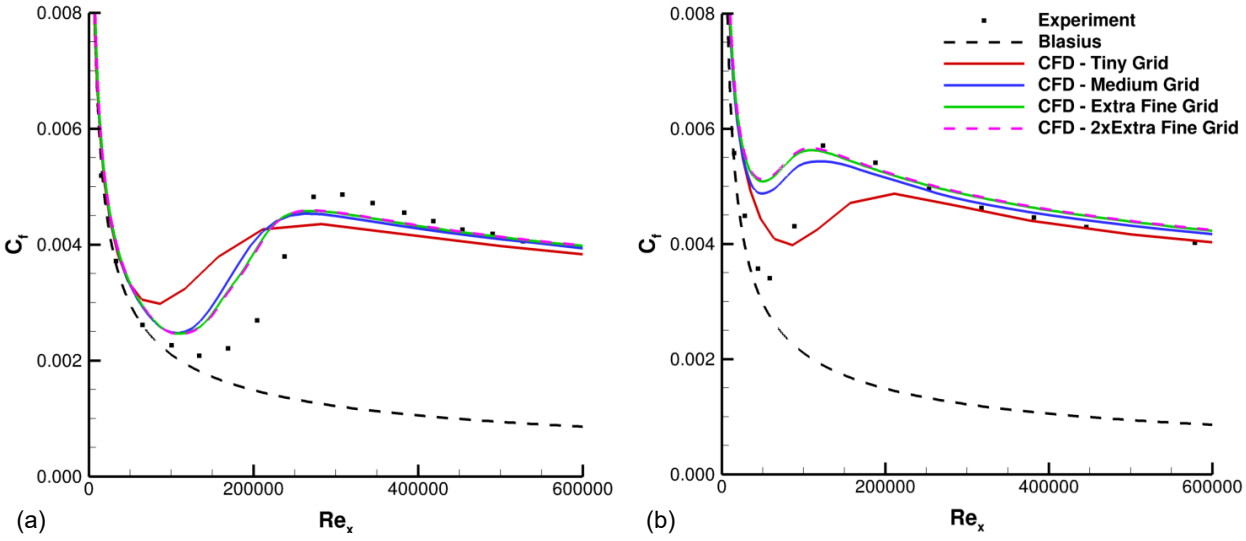


Figure 3.—2D flat plate skin friction coefficient profiles at the T3A (a) and T3B (b) conditions.

## 5.2 Axisymmetric Cone—Turbulence Parameter Study

A turbulence parameter study was performed on the coarsest grid level grid. This grid level was chosen because it was the cheapest computational grid to verify that each set of turbulence parameters would yield a converged solution. All simulations used the dissipative LDFSS flux construction scheme (Ref. 26) in conjunction with the van Leer flux limiter (Ref. 27) with a heuristic pressure limiter.

Equation (1) to (3) show how the inflow and cone tip stations are related, as a function of distance from the inflow domain to the leading edge of the cone, *s*.

$$k_{in} = 1.5 \times (M_\infty \times 0.01 \times I_{in})^2 \tag{1}$$

$$\omega_{in} = \frac{k_{in}}{\mu_t/\mu} = \left[\frac{\beta \times s}{u_{\text{tip}}} + \frac{1}{\omega_{\text{tip}}}\right]^{-1} \tag{2}$$

$$k_{in} = k_{\text{tip}} \times \left[\frac{\beta \times \omega_{\text{tip}} \times s}{u_{\text{tip}}} + 1\right]^{-\beta^*/\beta} \tag{3}$$

where

$$s = x_{in} - x_{\text{tip}} \tag{4}$$

$$u_{\text{tip}} = u_\infty \tag{5}$$

$$\beta = 0.0828 \tag{6}$$

$$\beta^* = 0.09 \tag{7}$$

With regards to the turbulence parameters, the inflow turbulence intensity was set to 1.25 percent, based on the recommendation from Reference 28 for the AETC tunnel B. These values were also used successfully for investigations of a simpler transition-sensitized RANS model in Reference 29. A broad range of inflow $\mu_t/\mu$, which effectively changes the turbulent length scale for a given turbulence intensity setting, were examined to gauge the effect of freestream turbulence settings on the predicted transition location. A wide range of turbulent viscosity ratios were selected, as shown in Table VI. It may be observed that the broad range in $\mu_t/\mu$ values results in a much smaller range in turbulence intensities at the cone tip, which is due to the nonlinearity of Equation (2) and (3). For a given turbulence intensity, a larger $\mu_t/\mu$ corresponds to a smaller turbulent dissipation rate, such that the inflow turbulence intensity of 1.25 percent will decay more slowly with increasing $\mu_t/\mu$.

The turbulent kinetic energy at the cone tip was determined by iterating on the value of $k_{\text{tip}}/k_{in}$ and inserting into Equation (3) until the turbulence intensity at the cone tip was converged upon. The turbulence intensity at the cone tip was then determined via Equation (8).

$$I_{\text{tip}} = \frac{1}{u_{\text{tip}}} \times \sqrt{\frac{2}{3} k_{\text{tip}}} \tag{8}$$

To aid in the convergence of the simulations, the flow was initialized as follows. A simulation was performed with the SA turbulence model where the flow was initialized with uniform flow at the run condition total pressure and total temperature. The converged SA turbulence model solution was then used to initialize the mean flow for a simulation that used the SST-V turbulence model. In turn, the converged SST-V turbulence model solution was then used to initialize the mean flow for a simulation that used the LM-SST transition model with an inflow $\mu_t/\mu$ of 5.0. The remaining LM-SST transition

model simulations were performed in order with increasing $\mu_t/\mu$ with each simulation initialized from the previous converged solution.

In the experiments, transition to turbulence was identified by measuring the surface heat transfer along the cone surface. Figure 4 shows the resultant Stanton number profiles plotted as a function of the boundary layer edge Reynolds number. The Stanton number was computed per Equation (9) and the boundary layer edge Reynolds number was based on the conditions downstream of the oblique shock, or in other words the local "freestream" conditions within the shock layer.

$$\mathrm{St} = \dot{q}_w \Big/ \Big( \rho_\infty \times u_\infty \times \big( h(T_0) - h(T_w) \big) \Big) \tag{9}$$

Figure 4 shows that the predicted transition location moves upstream as the inflow turbulence is increased, a trend that has been shown in the previous section as well as in other zero-pressure-gradient flat plate simulations (Ref. 30). This trend, however, is significant when considering the design of an inlet for a hypersonic vehicle as the transition location has a direct effect on the inlet performance. The results shown in Figure 4 demonstrates that by increasing the inflow $\mu_t/\mu$ from 50.0 to 400.0 leads to a decrease in the transition point Reynolds number based on the cone position and the boundary layer edge quantities by ~$3.53\times10^6$ (or equivalently a decrease in the nondimensional axial location $dx/L$ by 0.382). The transition point was defined as the Stanton number profile sharp increase midpoint. The finding of this sensitivity is significant as hypersonic inlet design often assumes a transition point and does not consider the sensitivity of that location to the incoming turbulence. It is also noted that the LM-SST transition model seems to best predict the transition location relative to the experiment with an inflow $\mu_0/\mu$ of 100.0 (corresponding to a turbulence intensity of 0.959 percent at the cone tip). By no means are these values suggested as global settings for other problems, but only the set of freestream turbulence parameters that enable closest replication of the experimentally observed transition location.

Aside from assessing the capability of the LM-SST transition model to predict transition, it is noted from Figure 4 that the SA and SST-V turbulence models also predicted transition, although much earlier than as predicted by the transition model and the experiment. One thing that caught the authors' attention was that the turbulence model simulations were predicting transition at a location corresponding to higher-than-expected boundary layer edge Reynolds numbers (~$1.92\times10^6$ for the SA turbulence model simulation and ~$1.54\times10^6$ for the SST-V turbulence model simulation). As discussed earlier, it is generally expected that RANS models without any specifics for transition modeling will experience a natural transition of sorts very near the origin of a boundary layer and usually at correspondingly very low equivalent Reynolds numbers. This peculiarity will be further explored by revisiting the zero-pressure-gradient flat plate at a range of Mach numbers later in this paper.

TABLE VI.—STUDIED TURBULENCE PARAMETER VALUES FOR THE AXISYMMETRIC CONE

| Inflow | | Cone tip |
|---|---|---|
| $\mu_t/\mu$ | $I$, % | $I$, % |
| 5.0 | 1.25 | 0.303 |
| 50.0 | 1.25 | 0.803 |
| 100.0 | 1.25 | 0.959 |
| 200.0 | 1.25 | 1.078 |
| 400.0 | 1.25 | 1.155 |

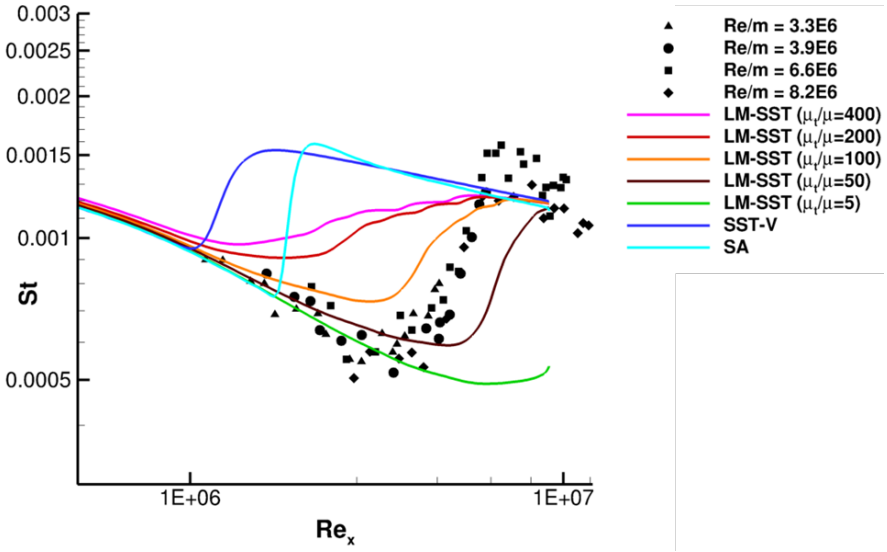


Figure 4.—Axisymmetric cone Stanton number profiles for the turbulence parameter study.

## 5.3 Axisymmetric Cone—Grid Convergence Study

For thoroughness, a grid convergence study was completed. The simulations used the same flux construction scheme, flux limiter, and flow initialization as the turbulence parameter study. For brevity, the grid convergence study was only performed for the SA turbulence model, SST-V turbulence model, and the LM-SST transition model with an inflow $\mu_t/\mu$ of 5.0 and 100.0. Figure 5 shows the Stanton number profiles plotted as a function of the boundary layer edge Reynolds number for the turbulence model simulations while Figure 6 shows the corresponding plots for the transition model simulations. It can be seen that the Stanton number profiles show near grid convergence on the medium level grid for the turbulence model simulations while extra refinement was required to reach grid convergence for the transition model simulations. To save computational expense, the finest grid, denoted as fine-c, only had refinement along the cone. Specifying the refinement in that region was based on the trend that the lack of grid convergence on the coarser grids was concentrated around the predicted transition location. The fine-c grid had $96.53\times10^6$ nodes (compared to the fine grid which had $75.37\times10^6$ nodes).

## 5.4 2D Flat Plate Revisited

As a result of the observation from the cone studies that the fully turbulent RANS simulations exhibited a transition location further downstream than expected, a freestream Mach number study was performed to gauge the sensitivity to the predicted transition location when using the SST model, using the vorticity-based turbulence production term (or SST-V model), in "fully turbulent" RANS mode. The simulations were performed on the extra fine grid level grid that was used for the low Mach number transition cases discussed earlier in this report as this grid was shown to be grid converged. The freestream Mach numbers explored included Mach 0.2, 1.0, 2.0, 4.0, 6.0, and 8.0, with nominal $y^+$ values shown in Table VII. The surface boundary conditions for the supersonic freestream Mach numbers were the same as the simulations for the freestream Mach number of 0.2, while the inflow and outflow boundaries were modified. Those boundary conditions were set to freestream at the inflow and extrapolated at the outflow. To compare against the FUN3D simulation results, a set of equivalent simulations were performed with the Wind-US code, also in fully turbulent RANS mode, but using a structured grid flow solver.

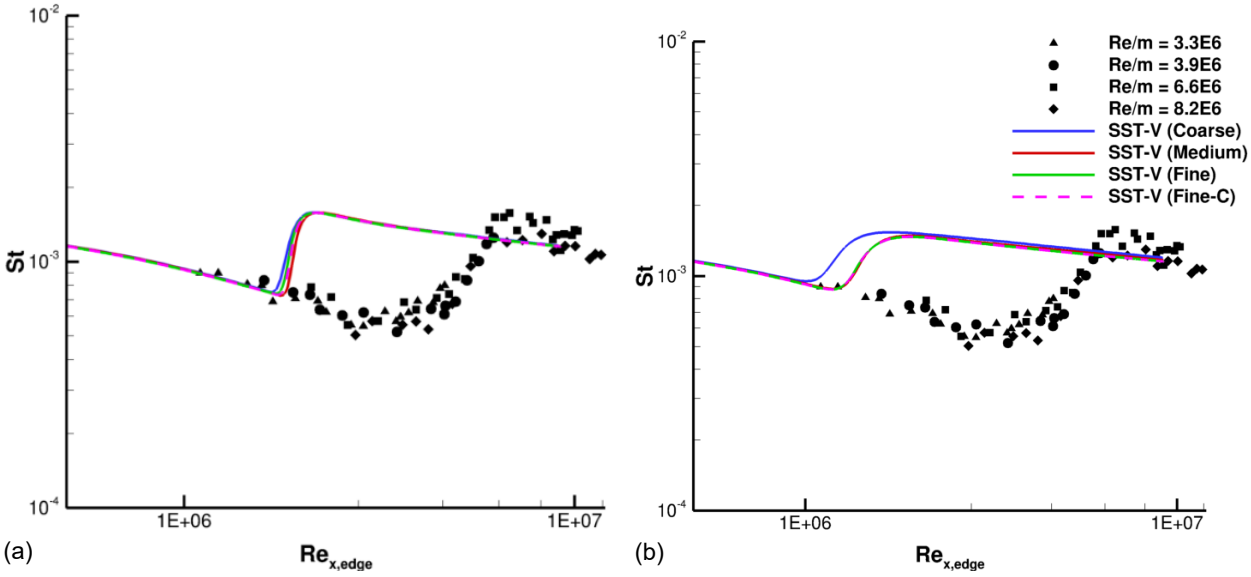


Figure 5.—Axisymmetric cone Stanton number profiles for the SA (a) and SST-V (b) turbulence model simulations.

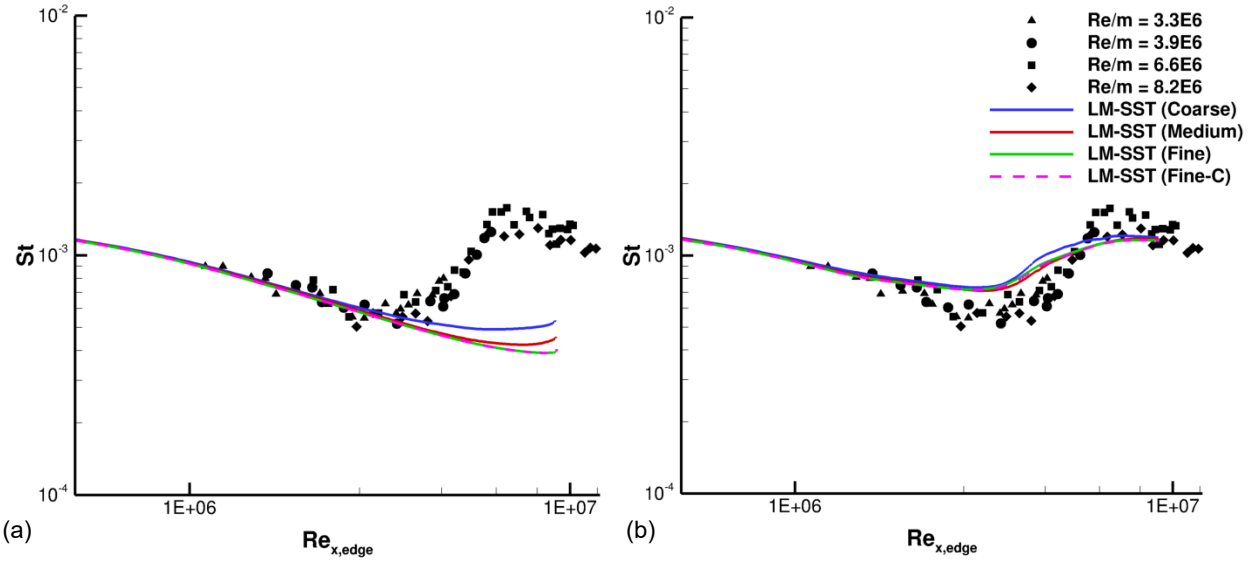


Figure 6.—Axisymmetric cone Stanton number profiles for the LM-SST transition model simulations with an inflow $\mu_t/\mu$ of 5.0 (a) and 100.0 (b).

Figure 7 shows the resulting skin friction coefficient profiles at the various freestream Mach numbers. For all conditions, the SST-V model and essentially all two-equation RANS turbulence models experience a transition of sorts, but this typically is expected early in the boundary layer development such that the flow can still be considered "fully turbulent." At low Mach numbers, as shown in Figure 7, this is verified to be the case with the SST-V model. Up to Mach 2.0, predictions using the two codes are nearly identical. It can be seen that the predicted transition location moves downstream as the freestream Mach number increases. This matches the trend shown by Rumsey (Ref. 31) who performed CFL3D simulations using the SST turbulence model. As the freestream Mach number is increased to four and

above, the difference in the numerical transition becomes larger between the two codes. All the cases considered here employed an adiabatic wall condition, except for one case at Mach 8.0 where an additional case was set where the wall temperature was set to the same ratio as that for the hypersonic cone of the previous section, in order to determine the effect of wall temperature state on the boundary layer transition performance of RANS models in fully turbulent mode.

For the Mach 8.0 adiabatic wall cases, Figure 7 shows the predicted transition location begins for the Wind-US simulation at approximately $8.0\times10^5$ while for the FUN3D simulation, the transition process begins much further downstream at $1.4\times10^6$. Fully turbulent mode is achieved for the Wind-US simulation at approximately $1.4\times10^6$ and for the FUN3D simulation at approximately $2.7\times10^6$. The Mach 8.0 case with the lower wall temperature that matches the cone case transitions significantly earlier that the adiabatic wall case and, as expected, results in a fully turbulent skin friction that is higher than that for the adiabatic wall case. It is only a coincidence that the skin friction for the Mach 8.0 case at the lower wall temperature is very similar to the skin friction coefficient of the Mach 6.0 adiabatic wall case downstream in the fully turbulent regime. Equating the Mach 8.0 cold wall flat plate case to a fully turbulent Reynolds number based on the conditions downstream of the oblique shock yields a value of $1.41\times10^6$, which is similar to the value predicted in the hypersonic cone simulations.

Briefly, the SA model was also investigated in fully RANS mode for these flat plate cases with variation in freestream Mach number, as shown in Figure 8. These calculations were only performed with Wind-US. It may be observed that there is a similar delay in boundary layer transition as the freestream Mach number increases, but only at the highest Mach numbers investigated, 6.0 and 8.0. Relative to the Wind-US solution with the SST-V turbulence model at Mach 8.0, the numerical transition with the SA turbulence model begins at a lower Reynolds number and also achieves a fully turbulent state more quickly. This matches the trend shown by Rumsey and Spalart (Ref. 32) who performed CFL3D simulations with the SA and SST turbulence models. While the original and still primary objective of this paper was to investigate a widely used transition-sensitized RANS model, these fully turbulent results indicate that there is a numerical transition process at higher freestream Mach numbers which may not be desired by an analyst when intending to run a RANS code in fully turbulent mode. A comprehensive study of the effect of freestream turbulence levels for these fully turbulent RANS simulations was not in the scope of this paper but would be worthwhile to be investigated to determine if the Mach number sensitivity is reduced or eliminated with other freestream turbulence settings.

TABLE VII.—NOMINAL 2D FLAT PLATE $y^+$ VALUES

| $M_\infty$ | $y^+$ |
|---|---|
| 0.2 | $9.72\times10^{-2}$ |
| 1.0 | $7.98\times10^{-2}$ |
| 2.0 | $5.07\times10^{-2}$ |
| 4.0 | $2.03\times10^{-2}$ |
| 6.0 | $1.01\times10^{-2}$ |
| 8.0 | $5.92\times10^{-3}$ |

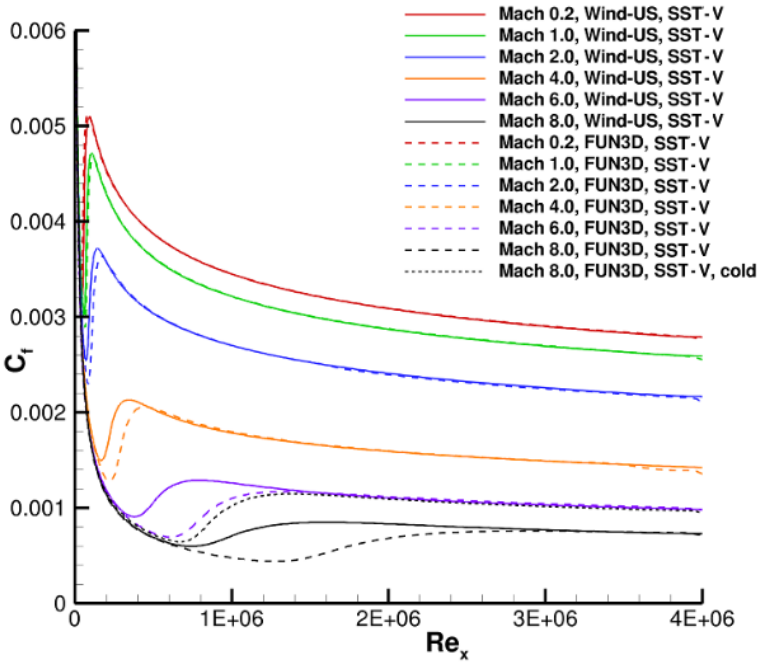


Figure 7.—2D flat plate skin friction coefficient profiles with varying freestream Mach numbers (SST-V turbulence model solutions).

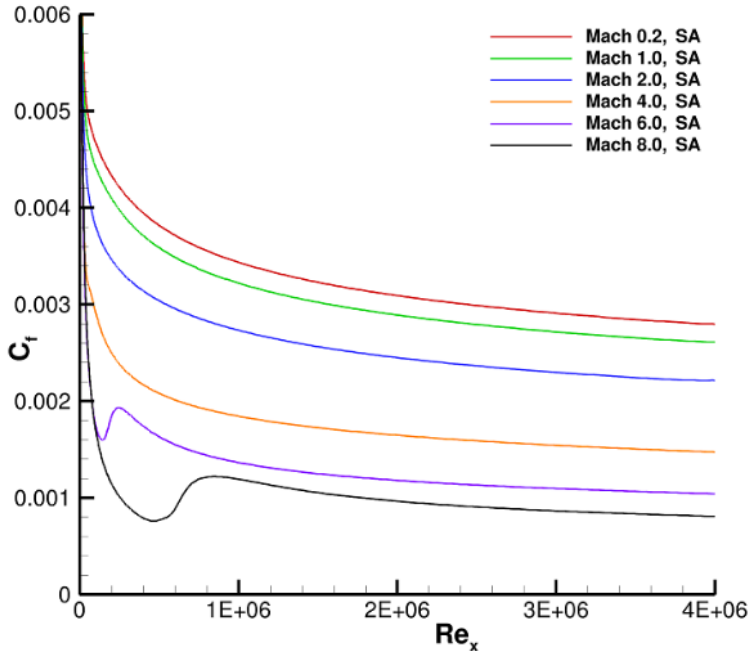


Figure 8.—2D flat plate skin friction coefficient profiles with varying freestream Mach numbers (Wind-US SA turbulence model solutions).

## 6.0 Conclusions

A series of steady-state simulations were performed to explore the use of a popular transition-sensitized RANS model for predicting transition for high speed applications. The focus transition problem was a hypersonic cone that would represent the forebody of a hypersonic vehicle, and hence the initial part of an inlet compression system. The Langtry-Menter Shear-Stress Transport (LM-SST) transition model as implemented in the FUN3D code was chosen for the study, and it was compared with results using the SA and SST-V turbulence models in fully turbulent mode. The investigations began with a baseline incompressible zero-pressure-gradient flat plate. The flat plate simulations showed that the transition model was able to reasonably predict the transition location at a freestream Mach number of 0.2.

An axisymmetric cone was examined next, and the simulations showed a significant sensitivity of the freestream turbulence on the predicted transition location. Comparisons of surface heat transfer were made between experimental data and computations obtained with the LM-SST transition model, and variations in freestream turbulence settings were examined. Determination of freestream turbulent settings in high Mach number experiments is frequently challenging, and even if a turbulence intensity can be identified, the setting for the turbulent length scale is typically not as easy to determine, yet required when using a two-equation RANS model as the basis for a transition simulation technique. Solutions for the cone indicated that a nearly grid-converged result could be obtained even for the high Mach number case.

For reference, the SST-V and SA RANS models in fully turbulent mode were also run for the cone case. Turbulence models operated in "fully turbulent" mode are usually expected to transition numerically very near the origin of the boundary layer but were noted during the cone simulations to transition much further downstream than expected. Therefore, another set of flat plate investigations were investigated where the Mach number was varied from 0.2 to 8 to more thoroughly investigate the transition behavior of RANS models in fully turbulent mode. The flat plate simulations showed that the predicted transition location moved downstream as the freestream Mach number was increased when using the SST-V turbulence model. This was an unexpected finding at first as the one- and two- equation models are usually assumed to produce fully turbulent flow from near the leading edge of a boundary layer simulation, however, this trend verified the trend seen in the cone simulation. For high speed flow investigations where the flow is assumed to be fully turbulent from the leading edge, the delayed transition behavior as exhibited here may result in incorrect predictions of overall viscous drag, as well as overall performance of an inlet. The trend observed with FUN3D was confirmed with simulations using the Wind-US code. While these results with two codes were obtained for the SST-V model, similar behavior was obtained with Wind-US when using the SA turbulence model. It was also shown that the predicted transition location for the axisymmetric cone when using the SST-V turbulence model compared well with the equivalent zero-pressure-gradient cold wall flat plate case.

## References


1. Gregg, R., "The Challenges of Certification by Analysis," Presented at the 13th Symposium on Overset Composite Grids and Solution Technology, Mukilteo, WA, 2016.
2. Slotnick, J. P., and Mavriplis, D. J., "A Grand Challenge for the Advancement of Numerical Prediction of High Lift Aerodynamics," AIAA-2021-0955, January 2021.
3. Slotnick, J. P., Khodadoust, A., Alonso, J., Darmofal, D., Gropp, W., Lurie, E., and Mavriplis, D., "CFD Vision 2030 Study: A Path to Revolutionary Computational Aerosciences," NASA/CR-2014-218178, March 2014.

4. "NASA Aeronautics Strategic Implementation Plan 2019 Update," NASA Aeronautics Strategic Implementation Plan, URL: https://www.nasa.gov/sites/default/files/atoms/files/sip-2019-v7-web.pdf [cited 10 April 2023].
5. Reshotko, E., "Transition Issues at Hypersonic Speeds," AIAA 2006-707, January 2006.
6. Langtry, R. B., and Menter, F. R., "Correlation-Based Transition Modeling for Unstructured Parallelized Computational Fluid Dynamics Codes," *AIAA Journal*, Vol. 47, No. 12, 2009, pp. 2894-2906.
7. Spalart, P., and Allmaras, S., "A One-Equation Turbulence Model for Aerodynamic Flows," *La Recherche Aerospatiale*, No. 1, 1984, pp. 5-21.
8. Menter, F. R., "Improved Two-Equation k-omega Turbulence Models for Aerodynamic Flows," NASA/TM-103975, October 1992.
9. Biedron, R. T., Carlson, J.-R., Derlaga, J. M., Gnoffo, P. A., Hammond, D. P., Jacobson, K. E., Jones, W. T., Kleb, B., Lee-Rausch, E. M., Nielson, E. J., Park, M. A., Rumsey, C. L., Thomas, J. L., Thompson, K. B., Walden, A. C., Wang, L., and Wood, W. A., "FUN3D Manual: 13.7," NASA/TM-2020-5010139, November 2020.
10. Yoder, D. A.., "Wind-US User's Guide Version 4.0," NASA/TM-2016-219145, September 2016.
11. Rumsey, C. L., and Lee-Rausch, E. M., "NASA Trapezoidal Wing Computations Including Transition and Advanced Turbulence Modeling," AIAA 2012-2843, June 2012.
12. Venkatachari, B. S., Denisen, M. F., Mysore, P.V., Hildenbrand, N. J., and Choudhari, M. M., "Toward Verification of the gamma-Re-theta Transition Model in OVERFLOW and FUN3D," AIAA-2022-3697, June 2022.
13. Papp, J. L., and Dash, S. M., "Rapid Engineering Approach to Modeling Hypersonic Laminar-to-Turbulent Transitional Flows," *Journal of Spacecraft and Rockets*, Vol. 42, No. 3, 2005, pp. 467-475.
14. Papp, J. L., and Dash, S. M., "Modeling Hypersonic Laminar to Turbulent Transitional Flows for 3D Geometries using Two-Equation Onset and Intermittency Transport Models," AIAA 2012-0449, January 2012.
15. Aliaga, C., Guan, K., Selvanayagam, J., Stokes, J., Viti, V., and Menter, F., "Hypersonic Applications of the Turbulent Transition SST Model in Ansys-Fluent," AIAA 2020-3290, June 2020.
16. Zhou, L., Zhao, R., and Yuan, W., "Applications of Improved k-ω-γ Transition Model to Hypersonic Complex Configurations," *AIAA Journal*, Vol. 57, No. 5, 2019, pp. 2214-2221.
17. You, Y., Luedeke, H., Eggers, T., and Hannemann, K., "Application of the γ-$Re_{\theta t}$ Transition Model in High Speed Flows," AIAA 2012-5972, September 2012.
18. Krause, M., Behr, M., and Ballmann, J., "Modeling of Transition Effects on Hypersonic Intake Flows Using a Correlation-Based Intermittency Model," AIAA 2008-2598, April 2008.
19. Guo, P., Gao, Z., Zhang, Z., Jiang, C., and Lee, C. H., "Local-Variable-Based Model for Hypersonic Boundary Layer Transitions," *AIAA Journal*, Vol. 57, No. 6, 2019, pp. 2372-2383.
20. "1st AIAA Transition Modeling and Prediction Workshop," January 2021. URL: http://transitionmodeling.larc.nasa.gov/workshop_i/.
21. Kimmel, R. L., "The Effect on Pressure Gradients on Transition Zone Length in Hypersonic Boundary Layers," AFLR Report WL-TR-94-3012, December 1993.
22. Pointwise, Software Package, Version 18.4 Release 4, Cadence Design Systems Inc., Fort Worth, TX, 2021.
23. Roe, P. L., "Approximate Riemann Solvers, Parameter Vectors, and Difference Schemes," *Journal of Computational Physics*, Vol. 43, No. 2, 1981, pp. 357-372.
24. Venkatakrishnan, V., "Convergence to Steady State Solutions of the Euler Equations on Unstructured Grids with Limiters," *Journal of Computational Physics*, Vol. 118, No. 1, 1995, pp. 120-130.

25. Roach, P. E., and Brierley, D. H., "The Influence of Turbulent Freestream on Zero Pressure Gradient Transitional Boundary Layer Development. Part 1: Testcases T3A and T3B," *Numerical Simulations of Unsteady Flows and Transition to Turbulence*, editors O. Pironneua, W. Rodi, and I. Ryhming, Cambridge University Press, 1992, pp. 319-347.
26. Edwards, J. R., "A Low-Diffusion Flux-Splitting Scheme for Navier-Stokes Calculations," *Computers & Fluids*, Vol. 26, No. 6, 1997, pp. 635-659.
27. Van Leer, B., "Towards the Ultimate Conservative Difference Scheme II. Monotonicity and Conservation Combined in a Second Order Scheme," *Journal of Computational Physics*, Vol. 14, No. 4, 1974, pp. 361-370.
28. McDaniel, R. D., and Hassan, H. A., "Role of Bypass Transition in Conventional Hypersonic Facilities," *39th AIAA Aerospace Sciences Meeting and Exhibit*, AIAA 2001-0209, January 2001.
29. Denissen, N.A., Yoder, D.A., and Georgiadis, N.J., "Implementation and Validation of a Laminar-to-Turbulent Transition Model in the Wind-US Code," NASA TM-2008-215451, September 2008.
30. Herbert, Th., Stuckert, G. K., and Esfahanian, V., "Effects of Free-Stream Turbulence on Boundary-Layer Transition," *31st Aerospace Sciences Meeting & Exhibit*, AIAA-93-0488, January 1993.
31. Rumsey, C. L., "Compressibility Considerations for $k$-$\omega$ Turbulence Models in Hypersonic Boundary-Layer Applications," *Journal of Spacecraft and Rockets*, Vol. 47, No. 1, 2010, pp. 11-20.
32. Rumsey, C. L., and Spalart, P. R., "Turbulence Model Behavior in Low Reynolds Number Regions of Aerodynamic Flowfields," AIAA-2008-4403, June 2008.